Provided for non-commercial research and education use.
Not for reproduction, distribution or commercial use.

Volume 255, No. 24 30 September 2009 ISSN 0169-4332

ELSEVIER

applied
surface science

A journal devoted to applied physics
and chemistry of surfaces and interfaces

Proceedings of the Sixth International Conference on
Photo-Excited Processes and Applications
(6-ICPEPA)

Guest editors:
Koji Sugioka
Aaron Peled

Volume 255, No. 24, pp. 9557–9908

30 September 2009

Available online at www.sciencedirect.com
ScienceDirect

This article appeared in a journal published by Elsevier. The attached copy is furnished to the author for internal non-commercial research and education use, including for instruction at the authors institution and sharing with colleagues.

Other uses, including reproduction and distribution, or selling or licensing copies, or posting to personal, institutional or third party websites are prohibited.

In most cases authors are permitted to post their version of the article (e.g. in Word or Tex form) to their personal website or institutional repository. Authors requiring further information regarding Elsevier's archiving and manuscript policies are encouraged to visit:

http://www.elsevier.com/copyright

Applied Surface Science 255 (2009) 9665–9670

Contents lists available at ScienceDirect

Applied Surface Science

journal homepage: www.elsevier.com/locate/apsusc

Towards laser-manipulated deposition for atom-scale technologies

F. Tantussi [a,b], V. Mangasuli [b], N. Porfido [b], F. Prescimone [b], F. Fuso [b], E. Arimondo [b], M. Allegrini [a,b,*]

[a] polyLab, INFM/CNR, Università di Pisa, Largo Pontecorvo 3, 56127 Pisa, Italy
[b] CNISM, Dipartimento di Fisica Enrico Fermi, Università di Pisa, Largo Pontecorvo 3, 56127 Pisa, Italy

ARTICLE INFO

Article history:
Available online 21 April 2009

PACS:
03.75.Be
39.25.+k
42.70.Qs

Keywords:
Atomic nanofabrication
Atom lithography
Laser manipulation
Tunneling microscopy

ABSTRACT

We have developed an apparatus for nanostructure fabrication based on direct deposition of laser-manipulated cesium vapors onto pyrolitic graphite. Key features of our apparatus are production and manipulation of a longitudinally cooled atom beam, which allows for straightforward operation in the moderate to low flux density conditions. Both unstructured and structured low surface coverage depositions have been carried out and samples carefully analyzed at the atom scale by in situ tunneling microscopy. Results represent a step forward to the realization of a novel technology for space-controlled deposition of few, eventually single, atoms.

© 2009 Elsevier B.V. All rights reserved.

1. Introduction

In the present scenario of nanotechnology, large efforts are being devoted to develop techniques for manipulating the dynamical properties of vapors at the single atom level. Such atom-scale technologies are expected to enable new fabrication schemes through direct deposition onto suitable substrates, with potential outcomes in a variety of applications, including, e.g., precision doped systems for spintronics, photonic band gap devices, integrated molecular/inorganics nanoelectronics.

Atom-scale technologies should fulfill two main requirements: (i) an accurate control of the dynamics (position, momentum, kinetic energy) of neutral species in the vapor phase; (ii) the possibility to transfer such control to samples composed of few, eventually single, atoms. Controlling the dynamical properties of atoms and molecules is one of the main achievements of atom optics [1], an area where many relevant advancements have been reported in the last decades. Application of atom optics to nanotechnology brought the development of atomic nanofabrication (ANF) [2,3], which originally was mostly conceived as a replacement to conventional (optical) lithography with the advantages of negligible diffraction effects and the use of immaterial masks.

We have developed an original apparatus for ANF where the atomic sample to be manipulated is a longitudinally laser-cooled atom beam [4] produced out of a modified magneto-optical trap (MOT); the beam is made of cesium, a species which, despite of poor direct technological exploitations, can be considered as a paradigm in laser manipulation owing to its simple electronic structure and availability of suitable laser sources. The most striking property of our beam is the sub-thermal character, meaning that atoms own a kinetic energy in orders of magnitude smaller than in conventional (effusive) beams.

The apparatus has been already successfully used in the conventional atom lithography implementation, where space segregation of the beam is used to impress a pattern onto a particle sensitive resist (alkylthiol self-assembled monolayers) grown on gold. Development and etching of the impressed pattern led to the fabrication of a regular nanotrench array in the substrate, with an average width around 45 nm [5].

Among the potential advantages offered by the laser-cooled beam, the ability to operate in well-controlled low flux conditions paves the route to depositions in moderate to low surface coverage regime. This paper addresses low coverage and low kinetic energy structured deposition of Cs onto highly oriented pyrolitic graphite (HOPG) and the in situ diagnostics at the atomic scale carried out by ultra-high vacuum scanning tunneling microscopy (UHV-STM) of the produced samples.

---

[*] Corresponding author at: Dipartimento di Fisica E. Fermi, Università di Pisa, I-56127 Pisa, Italy. Tel.: +39 0502214517; fax: +39 0502214333.
E-mail address: maria.allegrini@df.unipi.it (M. Allegrini).

0169-4332/$ – see front matter © 2009 Elsevier B.V. All rights reserved.
doi:10.1016/j.apsusc.2009.04.048

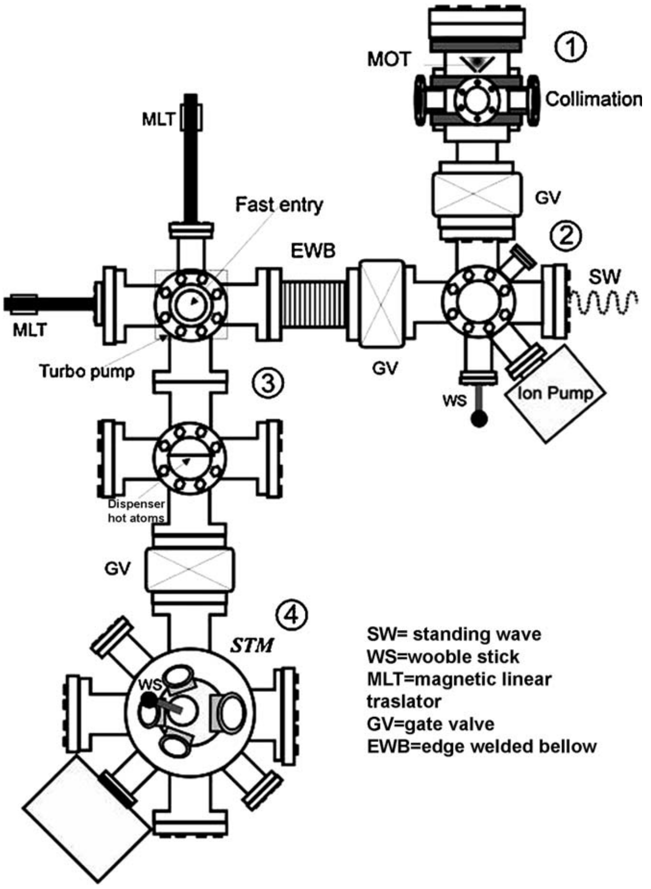

Fig. 1. Sketch of the UHV chamber: numbers in circles indicate the four different sections of the chamber, as discussed in the text. The system for the generation of the laser radiation needed to the experiment is not shown.

2. Experimental

The setup used in the present investigation has been already described elsewhere [4–6]. Basically, it is built around a UHV chamber (residual pressure $<10^{-9}$ mbar) divided into four regions, as schematically shown in Fig. 1. Core of the system is a modified MOT providing a continuous flow of laser-cooled Cs atoms following the interaction of a single laser beam and of a static quadrupolar magnetic field with background vapors produced by a pair of alkali metal dispensers (SAES Getters). The vapor is trapped and cooled down to a fraction of mK within a pyramidal-shaped arrangement of prisms and mirrors (pyramidal MOT); due to the presence of a small hole ($\sim$2 mm^2 area) at the pyramid apex, retro-reflection of the laser beam is prevented along the pyramid axis. Thus, transversally trapped and cooled atoms feel an unbalanced force along the axis and are pushed out of the pyramid forming a continuous beam. Right after the apex, the atoms enter a 2D transverse optical molasses region [7] made of two, mutually orthogonal, counterpropagating laser beams sent to cross the atoms at the right angle with the purpose to further reduce the transverse kinetic temperature of the atoms, therefore to provide a highly collimated atom beam. Radiation for the trapping and the 2D molasses operation is produced by two independent laser systems operating around 852 nm (quasi-resonant, red-detuned with respect to the D_2 Cs transition), based on diode lasers mounted in the master-slave configuration delivering up to $\sim$100 mW power. Master lasers are coupled to grating-ended external optical cavities in order to allow for tuning; the emission frequency is locked to Cs reference cells probed in the Doppler-free configuration. Additional radiation required for laser manipulation of Cs atoms (repumping radiation [7]) is provided by a distributed Bragg reflector (DBR) laser.

Thanks to a careful adjustment of the operating parameters, the system is able to produce a continuous beam of Cs atoms with a maximum flux above 10^9 atoms/s on a transverse size $\sim$4 mm full-width half-maximum (FWHM), being its residual divergence on the order of a few mrad [6]. The longitudinal velocity is around 10 m/s, according to optical time of flight measurements [4], with a translated Maxwellian velocity distribution $\sim$1.5 m/s wide. Correspondingly, the longitudinal kinetic temperature of the beam can be estimated in the tens of mK range, whereas the transverse temperature, as deduced from the divergence, is well below 1 mK.

The beam production and conditioning stages are followed by the deposition region, where the atoms are made to cross a 1D standing wave produced by an additional laser diode system whose radiation, with a power in the 30–60 mW range, is backreflected by a dielectric mirror placed in the vacuum chamber. Typically, the standing wave detuning with respect to the D_2 Cs resonance is around 1 GHz (toward the blue) and the beam is focused right above the substrate surface by either cylindrical or spherical converging lenses. The waist of the focal spot along the longitudinal axis of the atom beam is on the order of 100 μm (FWHM), leading to an interaction time in the several μs range. Special care has been devoted to design and realize a specific sample holder, ensuring correct and stable mutual alignment of the substrate surface, the standing wave, and the atom beam; moreover, a system based on a couple of high sensitivity CCD cameras looking at the sample along orthogonal directions has been implemented in order to detect the fluorescence emission from the Cs beam, hence to roughly locate the expected position of the structured deposit onto the substrate.

The UHV chamber is completed by two more sections devoted to fast entry load lock (to replace the substrate) and to sample diagnostics, respectively. Chamber regions are separated by gate valves and a system of UHV translators allows for sample manipulation in-vacuum. Diagnostics is accomplished by a UHV-STM head (Omicron LS-STM) controlled by commercial electronics (Nanotec Dulcinea with WSxM software [8]).

The substrates used for the present investigation are freshly peeled ZYA-grade HOPG surfaces (purchased from μ-Masch); choice of such a material has been motivated by the possibility to obtain relatively large atomically flat regions by ex situ removal of the uppermost graphene layers. Deposition and STM analysis of the samples have been accomplished at room temperature.

3. Basic manipulation mechanism

The key mechanism of ANF relies on the occurrence of a conservative force, the so-called dipolar force [7], occurring when a well-collimated beam of atoms crosses a standing wave quasi-resonant with an atomic transition. Dipolar forces can be interpreted within either classical [2,7] or semiclassical [9,10] pictures; in both cases, a net force turns to be exerted on the atoms oriented along the k-vector of the standing wave (considered here as the X-axis; we will assume the atom beam moving along the Z-axis of the same reference system). In particular, the classical interpretation leads to the following approximate expression for the force $F(x)$ [2]:

$$F(x) \approx -\frac{\hbar\Gamma^2}{8\delta I_S}\frac{\partial I(x)}{\partial x} \tag{1}$$

where Γ is the inverse of the natural lifetime and I_S the saturation intensity of the considered transition ($\Gamma \sim 2\pi \times 5.2$ MHz, $I_S \sim 1.1$ mW/cm^2), δ is the detuning and $I(x)$ is the intensity distribution of the standing wave radiation.

According to Eq. (1), the sign of the force depends on the gradient of the field intensity; assuming a 1D standing wave, atoms are then guided towards nodes (or antinodes, depending on the sign of δ) of the field. As a consequence, a spatially homogeneous beam turns out segregated, giving rise to a nanosized patterning which is reflected into the deposition of a nanostructured pattern onto the substrate.

In the conventional implementations of ANF [2], where thermal (effusive) beams are used, the relatively short interaction time experienced by the atoms rapidly moving in the standing wave field leads to atom focusing effects: most of the beam is focused in a small spot, whose transverse size is limited mainly due to spurious phenomena (e.g., the atom optics analogous of chromatic and spherical aberrations). Usually, the depth of focus for the considered focusing mechanism is very short, that makes rather cumbersome adjusting and controlling the relative distance between standing wave and substrate. Note, however, that diffraction plays a negligible role: as a matter of fact, the de Broglie wavelength of an atom beam ($\lambda_{\mathrm{dB}} = h/p$, with h the Planck's constant and p the atom momentum), ruling diffraction effects, is well below 1 nm.

Thanks to the use of a laser-cooled beam, in our experiment the interaction time is long enough to produce several transverse oscillations of the atoms moving in the standing wave field. Consequently, the so-called channeling regime is accessed, meaning that the initially homogeneous atom beam is segregated in parallel planes with $\lambda/2$ spacing (λ = 852 nm). Depth of focus in this regime is by far less critical and the role of background (unfocused) atoms is expected to be less prominent with respect to the focusing regime.

Monte Carlo simulations of the atom trajectories based on the complete semiclassical approach, to be presented in a forthcoming paper, demonstrate that efficient channeling can be achieved in our experimental conditions: beam patterning is realized with a $\lambda/2$ periodicity, even though, in agreement with [10], exotic periodicities (e.g., $\lambda/4$, $\lambda/8$) cannot be completely neglected in specific conditions of standing wave intensity and initial divergence of the beam.

The role of divergence, hence the need for collimation, can be understood also in terms of energy. The inhomogeneous field of the standing wave produces an array of potential wells along the X direction; in order for the atoms to be efficiently guided, their kinetic energy associated with the motion along the same axis must be well below the depth of the potential well, which, in turn, depends on the field intensity. A rough estimation based on $F(x) = -\bigtriangledown U(x)$, with $F(x)$ given in Eq. (1) and $U(x)$ space-dependent potential, suggests an height of the potential wells on the order of hundreds of neV, to be compared with the tens of neV of the transverse kinetic energy in our experiment. It is therefore clear that application of the technique to atom beams with a larger initial divergence, as, for instance, those created by laser ablation in the presence of a carrier gas (supersonic beams), would require a correspondingly larger power in the standing wave.

4. Results and discussion

In the experiment of Ref. [5], used to firstly assess the technique, the flux density of the atom beam and the duration of the deposition were adjusted in order to achieve impression of the particle-sensitive molecular resist, the dose being 2–4 atoms per molecule [2,5]. Direct deposition experiments discussed here are, on the contrary, carried out in the low surface coverage regime. There are no well-established conventions to define the surface coverage θ for Cs on HOPG, mainly due to the variety of structural variants reported in the relevant literature [11]; we will hereafter refer θ to the surface density of the carbon atoms forming the uppermost graphene layer ($\sim 38 \times 10^{14}$ atoms/cm^2) and we will define $\theta = 1$ (i.e., 1 monolayer) when an equal number of Cs atoms impinges onto a unit area of the HOPG substrate. We note that, such a definition underestimates the actual coverage when regular lattice phases, e.g., the ($\sqrt{3} \times \sqrt{3}$), the ($\sqrt{7} \times \sqrt{7}$), or the $p(2 \times 2)$, all reported in the literature [11], are formed.

Unless otherwise stated, samples considered in this paper have been typically produced with a Cs coverage in the range $\theta = 0.05$–0.20, attained with an atom flux $\sim(1–5) \times 10^8$ atoms/s (measured through optical spectroscopy) and with a deposition time in the tens, or hundreds, of minutes range. In our evaluation of θ we have duly taken into account the local enhancement of the atom flux density due to the atom guiding effect; the enhancement factor can be estimated as 5–10, depending on the operating parameters [6].

We stress that the use of a modified MOT as the beam source allows for rather controlled operation also in moderate to low flux conditions. In fact, contrary to conventional (effusive) sources, the temperature and the divergence of our beam are determined by specific trapping and cooling mechanisms, hence the dynamical features of the atoms composing the beam are not spread in a wide range of values as in thermal beams. Work is presently in progress to characterize the beam in the low and very low flux conditions by high sensitivity optical spectroscopy.

4.1. Unstructured depositions

Fabrication of isolated nanostructures through low coverage deposition is heavily affected by a number of surface physics phenomena, including, for instance, particle diffusion, nucleation and growth [12]. Moreover, since the experiments are carried out at room temperature, diffusion of Cs atoms in the layered structure of HOPG (intercalation) cannot be ruled out [11]. As a matter of fact, deposition of Cs onto HOPG is frequently accomplished at cryogenic temperatures [13], expected to reduce both intercalation and re-evaporation of material, the latter favored by the vapor pressure typical of Cs. However, the literature reports also on room temperature depositions [11,14], where coexistence of disordered and ($\sqrt{3} \times \sqrt{3}$) phases has been observed. The nature of the Cs–C bond is still under debate, but the marked tendency to lose the outer electron customary in alkali atoms suggests charge image-promoted electron transfer processes leading to semi-ionic bonds [11]. Previous results based on high resolution STM imaging [6] indicate that single Cs atoms preferentially sit on the graphite hollow-site in the initial stage of Cs structure formation.

In order to check for fabrication and stability of isolated Cs structures onto HOPG, we have carried out preliminary experiments by non-structured thermal vapor deposition. To this aim, we have installed a Cs dispenser in an auxiliary region of our UHV system (see Fig. 1) and placed the substrate in front of the dispenser, at $\sim$10 mm far from its vapor emitting side, for predefined time intervals. We remark that no precise evaluation of the coverage can be given in such conditions, due to the highly inhomogeneous and divergent vapor distribution concerning the substrate. A rough estimate suggests $\theta \sim 0.1$ for a few minute deposition (at I = 3 A dispenser current).

Fig. 2(a) shows as an example the UHV-STM topography image of a so-deposited sample; in this image, as well as in all others presented in the following, we attribute the observed features to Cs owing to the absence of analogous features in bare substrates (prior to exposure to the Cs vapor). Isolated Cs structures were indeed observed; remarkably, no specific morphology was discerned in the grown islands, which appeared rather irregular in shape ("droplet-like" shape), possibly as a consequence of the wetting properties of Cs. We could not detect any lattice phase in

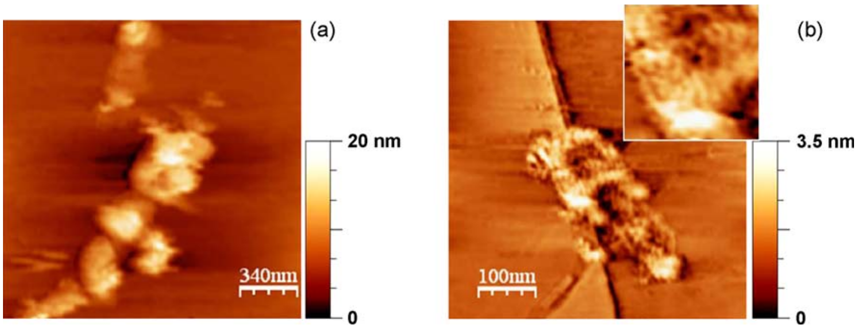

Fig. 2. UHV-STM topography images of unstructured Cs deposits on HOPG: sample produced by exposing the substrate to the vapor produced by a dispenser (a) and by direct deposition from the laser-cooled beam without the standing wave (b); in the inset: magnified scan (180 nm × 180 nm) over a Cs island. Estimated coverage is $\theta > 0.5$ and $\theta \sim 0.02$ for panels (a) and (b), respectively.

high resolution images, as a consequence either of the relatively large surface roughness (around 5 nm over a 100 nm^2 area) or due to the occurrence of a disordered phase, in agreement with [14].

Fig. 2(b) refers instead to a deposition from the laser-cooled beam; in this case, the standing wave was switched off in order to achieve unstructured deposition and the duration of the experiment was increased accordingly (the estimated corresponding coverage was $\theta \sim 0.02$). When imaged by UHV-STM, the sample surface appeared mostly free of any deposit, but for a few regions showing islands. Such regions were typically found close to graphite steps (the straight lines in the image), in particular at the intersection of different steps for the scan in Fig. 2(b). The explanation is straightforward [11,12]: graphite steps, naturally occurring during the peel-off procedure adopted to attain a fresh surface prior to deposition, act as nucleation sites for Cs growth. Diffusion is obviously involved in the process and atoms diffusing over the surface are collected during the growth.

Magnified scans of the Cs islands, as shown for instance in the inset of Fig. 2(b), revealed sub-structures sized in the tens, or few tens, of nm range. No clear evidence of regular phases was achieved also in this case, and the morphology appeared rather irregular, similar to the analogous structures produced in thermal conditions [see, e.g., Fig. 2(a)]. Therefore, the role of the kinetic energy of the impinging species can be assumed negligible, as expected taking into account the substrate temperature, much larger than that of the impinging species. Work is presently in progress to implement a substrate cooling stage: depositions in cryogenic conditions are expected to reduce effects of diffusion as well as of intercalation, which, according to the literature [15], could produce rather complicated effects in STM investigations.

4.2. *Structured depositions*

According to the numerical simulations (see Section 3), in the presence of the standing wave the beam gets space segregated in the form of an array of parallel planes, with $\lambda/2$ main periodicity and thickness on the order of few tens of nm. Obviously, such simulations do not consider any surface phenomena, which, instead, have been shown strongly involved in the growth process. Moreover, detection of the expected regular pattern produced in low coverage conditions is technically cumbersome because of the need to catch in a single scan nm-sized isolated features, consisting of a few atoms, and the ~426 nm periodicity. Rather than imaging the surface topography, the analysis can be conveniently carried out by acquiring maps of the tunneling current during the scan. Besides topography variations, tunneling current is known to be sensitive on the surface workfunction, depending in turn on the adsorption of material (the workfunction decreases when a monolayer of alkali atoms is deposited onto graphite [12,16]). Even though such an approach does not allow to properly describe the structure morphology, its enhanced sensitivity helps in detecting regular structures in large-scale scans.

Fig. 3(a) reports as an example the tunneling current map built during the scan of a sample deposited at an estimated coverage $\theta \sim 0.05$ in the presence of the standing wave (scan size 4 µm × 4 µm—the topography of the same region, not reported here, is much less defined and rather unclear): spots in the map can be attributed to isolated Cs nanostructures consisting of a few atoms. Most of the observed spots are organized to form lines, mutually parallel and spaced around $\lambda/$

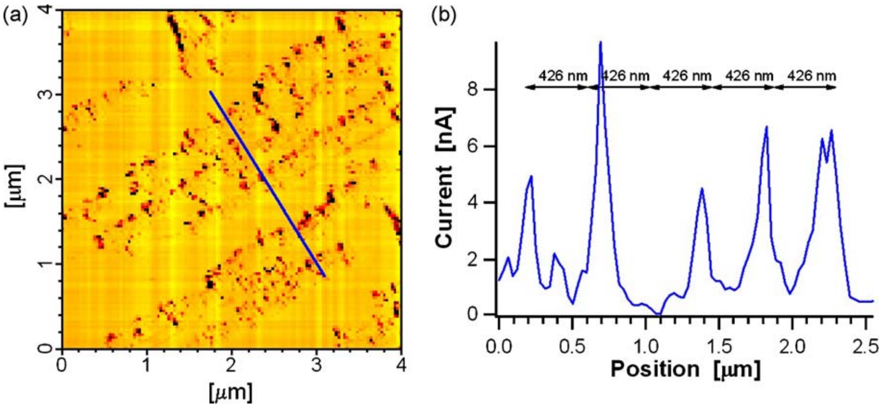

Fig. 3. UHV-STM current map on a sample produced by structured direct deposition at an estimated coverage $\theta \sim 0.05$ in the presence of the standing wave (a); profile analysis along the straight line superposed to the map (b).

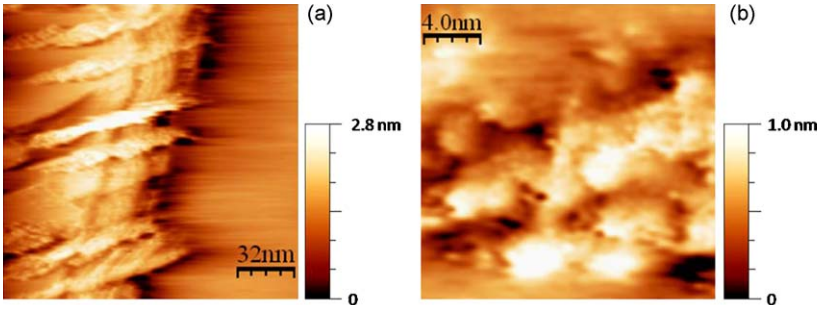

Fig. 4. UHV-STM topography images of structured Cs deposits on HOPG produced at an estimated coverage $\theta \sim 0.15$ by direct deposition in the presence of the standing wave: scan size 160 nm × 160 nm (a) and 20 nm × 20 nm (b).

2 = 426 nm, as demonstrated by the profile analysis in Fig. 3(b). Direction of the lines is well in agreement with the experimental geometry: in fact, they are orthogonal to the k-vector direction of the standing wave. Hence, the $\lambda/2$-spaced aligned spots, not observed in bare substrates, can be interpreted as representative of Cs nanolines produced by ANF in the low surface coverage regime.

It must be noted, however, that spots are observed also outside the expected positions and that, moreover, nanolines are not homogeneously distributed on the surface, at least in the considered scan. We cannot exclude technical problems (mechanical drifts, vibrations, other sources of noise) affecting the position of the nodes of the standing wave relative to the substrate, which might destroy the expected regularity of the pattern, even though long-term stability of the system has been assessed through optical interferometry [6]. We stress that the low flux density used in the experiment (estimated coverage $\theta \sim 0.05$) obviously leads to inhomogeneous material distribution on the surface, which, in turn, points at the role-played by the substrate (i.e., presence of atomic steps or other defects as nucleation sites) and by the associated surface physics phenomena involved in the process.

Relevance of the substrate, and in particular of the steps defining graphite terraces, is quite evident also in the image shown in Fig. 4(a), that refers to a sample deposited at an estimated coverage $\theta \sim 0.15$. In this case, we were not interested in detecting large-scale regularities and the small size of the scan (160 nm × 160 nm) allowed us to reliably map the surface topography. Elongated, cigar-shaped nanostructures are clearly seen, with their long axis orthogonal to the k-vector direction of the standing wave [note that, the sample is different with respect to Fig. 3(a), and so is the relevant angle]. Remarkably, the elongated structures were found only on substrate portions interested by the occurrence of graphite lattice steps. More specifically, Cs deposits were typically absent, or scarcely formed, on the flat top of HOPG terraces [see, e.g., the right side of the scan in Fig. 4(a)], whereas stable structures were found "across" different terraces (in the image, steps corresponding to 3–4 HOPG lattice steps are detected, with a total height variation around 1 nm). The finding can again be explained assuming particle diffusion controlled by potential barriers (the Ehrlich–Schwoebel barrier [17,18]), whose role in defining the morphology of atomic nanofabricated structures has been already pointed out through theoretical simulations [19]. Height and transverse width of the cigar-shaped structures are typically in the few nm and tens of nm range, respectively, whereas their length, clearly depending on the features of the underlying substrate, has been found in the 20–200 nm range.

The cigar-shaped islands exhibit an apparently continuous morphology; magnified scans, as shown for instance in Fig. 4(b), revealed nm-sized sub-structures whose height corresponds to the piling-up of 3–5 Cs atoms (assuming the Cs covalent radius ~ 0.22 nm). Due to the occurrence of sub-structures, attempts to unravel the lattice phase of the Cs deposits failed and we were not able to confirm either their regular or amorphous nature.

Remarkably, the direction of the long axis in all cigar-shaped structures detected and in all scanned samples was strictly related to the standing wave direction, while resulting rather independent of the HOPG lattice step orientation. This can be considered as a definite proof of the role-played by the standing wave in guiding atoms and, as a consequence, in defining the nanostructure morphology. Furthermore, in agreement with the above discussed results (see, e.g., Fig. 3 and Ref. [5]), the standing wave affects the large-scale spatial distribution of the deposited material: a more detailed analysis accomplished through a step-and-repeat STM imaging procedure, to be presented in a forthcoming paper, demonstrates that the production of the cigar-shaped nanostructures is space modulated with the $\lambda/2$ periodicity imposed by the standing wave. However, it must be noted that, as clearly seen also in Fig. 4(a), more than one Cs cigar is observed in a 160 nm scan, meaning that the position of the grown nanostructure is not completely governed by the standing wave: "satellites" are indeed seen in the scan (a careful analysis excluded as due to tip-related artifacts), with a mutual spacing on the order of few tens of nm. Further work is in progress to correlate this spacing with the possible exotic periodicities produced by the standing wave (see Section 3).

5. Conclusions

We have studied the room temperature production of Cs nanostructures on HOPG through deposition from a laser-cooled atom beam in the presence of laser guiding effects. Results indicate that stable isolated Cs structures, with a peculiar cigar-like morphology, can be fabricated, with transverse size in the 10 nm range, or below. The role of laser manipulation has been demonstrated: space distribution of the deposited atoms is partially modulated according to the standing wave periodicity, shape and orientation of the nanoislands are strictly connected with the standing wave direction. Relevant surface physics phenomena (e.g., diffusion and edge potential barriers) contribute to determine the nanostructure growth, which takes place only close to HOPG lattice steps.

Further work will be addressed to unravel such an interplay between the dynamical properties of the deposited vapor and the substrate features, from both the theoretical and the experimental points of view, in order to fully explore the potential of atom-scale technologies in the controlled fabrication of nanostructures made of a few isolated atoms.

Acknowledgment

Financial support from Fondazione Cassa di Risparmio di Pisa (PR 05/137) is gratefully acknowledged.

References

[1] P. Meystre, Atom Optics, Springer, New York, 2001.
[2] For a review, see: D. Meschede, H. Metcalf, J. Phys. D: Appl. Phys. D 36 (2003) R17; M.K. Oberthaler, T. Pfau, J. Phys.: Condens. Matter 15 (2003) R233.
[3] For a comprehensive list of references on atom optics based nanofabrication, see: B. Rohwedder, Am. J. Phys. 75 (2007) 394.
[4] A. Camposeo, A. Piombini, F. Cervelli, F. Tantussi, F. Fuso, E. Arimondo, Opt. Commun. 200 (2001) 231.
[5] C. O'Dwyer, G. Gay, B. Viaris de Lesegno, J. Weiner, A. Camposeo, F. Tantussi, F. Fuso, M. Allegrini, E. Arimondo, Nanotechnology 16 (2005) 1536.
[6] F. Tantussi, A. Camposeo, M. Alderighi, N. Puccini, E. Andreoni, M. Allegrini, E. Arimondo, F. Fuso, Mater. Sci. Eng. C 27 (2007) 1418.
[7] H. Metcalf, P. van der Straten, Laser Cooling and Trapping, Springer, New York, 2001.
[8] I. Horcas, R. Fernandez, J.M. Gomez-Rodriguez, J. Colchero, J. Gomez-Herrero, A.M. Baro, Rev. Sci. Instrum. 78 (2007) 013705.
[9] J. Dalibard, C. Cohen-Tannoudji, J. Opt. Soc. Am. B 2 (1985) 1707.
[10] D. Jurgens, A. Greiner, R. Stutzle, A. Habenicht, E. te Sligte, M.K. Oberthaler, Phys. Rev. Lett. 93 (2004) 237402.
[11] M. Caragiu, S. Finberg, J. Phys.: Condens. Matter 17 (2005) R995.
[12] J.A. Venables, Surface and Thin Film Processes, Cambridge University Press, Cambridge, 2000.
[13] A. Fubel, M. Zech, P. Leiderer, J. Klier, V. Shikin, Surf. Sci. 601 (2007) 1684, and references therein.
[14] Z.P. Hu, N.J. Wu, A. Ignatiev, Phys. Rev. B 33 (1986) 7683.
[15] M.-H. Whangbo, W. Liang, J. Ran, S.N. Magonov, A. Wawkuschewski, J. Phys. Chem. 98 (1994) 7602.
[16] M.T. Johnson, H.I. Stamberg, H.P. Hughes, Surf. Sci. 178 (1986) 290.
[17] G. Ehrlich, F.G. Hudda, J. Chem. Phys. 44 (1966) 1039.
[18] R.L. Schwoebel, E.J. Shipsey, J. Appl. Phys. 37 (1966) 3682.
[19] F. Nita, A. Pimpinelli, J. Appl. Phys. 97 (2005) 113529.